Giant surfactants provide a versatile platform for sub-10-nm nanostructure engineering

Xinfei Yu[a,1], Kan Yue[a,1], I-Fan Hsieh[a], Yiwen Li[a], Xue-Hui Dong[a], Chang Liu[a], Yu Xin[a], Hsiao-Fang Wang[b], An-Chang Shi[c], George R. Newkome[a], Rong-Ming Ho[b], Er-Qiang Chen[d,2], Wen-Bin Zhang[a,2], and Stephen Z. D. Cheng[a,2]

[a]Department of Polymer Science, College of Polymer Science and Polymer Engineering, University of Akron, Akron, OH 44325-3909; [b]Department of Chemical Engineering, National Tsing Hua University, Hsinchu 30013, Taiwan; [c]Department of Physics and Astronomy, McMaster University, Hamilton, ON, Canada L8S 4M1; and [d]Department of Polymer Science and Engineering, College of Chemistry and Molecular Engineering, Peking University, Beijing 100871, China

Edited* by Monica Olvera de la Cruz, Northwestern University, Evanston, IL, and approved May 2, 2013 (received for review February 8, 2013)

The engineering of structures across different length scales is central to the design of novel materials with controlled macroscopic properties. Herein, we introduce a unique class of self-assembling materials, which are built upon shape- and volume-persistent molecular nanoparticles and other structural motifs, such as polymers, and can be viewed as a size-amplified version of the corresponding small-molecule counterparts. Among them, "giant surfactants" with precise molecular structures have been synthesized by "clicking" compact and polar molecular nanoparticles to flexible polymer tails of various composition and architecture at specific sites. Capturing the structural features of small-molecule surfactants but possessing much larger sizes, giant surfactants bridge the gap between small-molecule surfactants and block copolymers and demonstrate a duality of both materials in terms of their self-assembly behaviors. The controlled structural variations of these giant surfactants through precision synthesis further reveal that their self-assemblies are remarkably sensitive to primary chemical structures, leading to highly diverse, thermodynamically stable nanostructures with feature sizes around 10 nm or smaller in the bulk, thin-film, and solution states, as dictated by the collective physical interactions and geometric constraints. The results suggest that this class of materials provides a versatile platform for engineering nanostructures with sub-10-nm feature sizes. These findings are not only scientifically intriguing in understanding the chemical and physical principles of the self-assembly, but also technologically relevant, such as in nanopatterning technology and microelectronics.

giant molecules | shape amphiphiles | hybrid materials | microphase separation | colloidal particles

Physical properties of materials are dictated by the hierarchical arrangements of atoms, molecules, and supramolecular assemblies across different length scales. The construction and engineering of structures at each length scale, especially at the 2- to 100-nm scale (1), are critically important in achieving desired macroscopic properties. As the traditional top–down lithography techniques face serious challenges in fabricating 2D and 3D nanostructured materials with sub-20-nm feature sizes (2), the bottom–up approach based on self-organization or directed assembly of functional molecules provides a promising alternative. The past decades have witnessed the development of diverse self-assembly building blocks ranging from small-molecule surfactants (3), block copolymers (4), and dendrimers (5) to DNAs (6, 7), peptides (8), and proteins (9). Notably, these motifs have enabled the programmed self-assembly of nanomaterials as demonstrated in DNA-coated nanoparticles (10–13). These studies have greatly improved our understanding of the thermodynamics and kinetics of self-assembly processes and opened enormous possibilities in modern nanotechnology.

Noncovalent interactions, such as hydrogen bonding, amphiphilic effect, π–π interaction, metal coordination bonding, and electrostatic forces, are known to be the fundamentals to precise self-assembly (14–16). Specific recognition and binding events, such as DNA hybridization and protein folding, are based on collective and cooperative multiple secondary interactions. More recently, anisotropy in shape has also been recognized as a critical factor in the self-assembly process due to packing constraints (17–22), as indicated by the emerging concept of "shape amphiphiles" (23, 24). However, it remains challenging to design nanomaterials "from scratch" (25) that can generate diverse structures at a specific length scale, e.g., the nanostructures with feature sizes around 10 nm or smaller.

Small-molecule surfactants have been a classic type of self-assembling materials and are typically composed of polar ionic heads and flexible hydrophobic tails. Although a variety of nanostructured assemblies can be created, they usually lack the required etching contrast between the hydrophobic and hydrophilic domains. The well-established microphase separation of block copolymers (26) has, on the other hand, led to the development of the block copolymer lithography, affording access to nanopatterning with high patterning density at low processing costs (27). Substantial progress has been demonstrated to guide the nanostructure formation in the block copolymer thin films at a 20- to 100-nm feature size scale. Pushing the feature sizes to an even smaller scale has given limited success (28). It is difficult to achieve a strong segregation with a sharp interface at sub-20-nm length scale, because the chemical incompatibility in typical block copolymers is reflected by the product of the interaction parameters χ and the degree of polymerization N (26). It is even more challenging to generate unconventional patterns, such as rectangular lattices (29), due to their thermodynamic metastability. Herein, we demonstrate size amplification and structural diversification of self-assembling small-molecule surfactants, as an effective strategy for the molecular design of a unique class of self-assembling "giant surfactants". This class of giant surfactants bridges the gap between small molecule amphiphiles and amphiphilic block copolymers and possesses advantages of both materials, thus providing a unique platform for engineering versatile nanostructures with sub-10-nm feature sizes.

Giant surfactants are precisely defined amphiphilic macromolecules that capture the essential structural features of the corresponding small-molecule surfactants, but at larger sizes (30). They are fundamentally more versatile, owing to the numerous possibilities for precise structural modification. Giant surfactants

Author contributions: E.-Q.C., W.-B.Z., and S.Z.D.C. designed research; X.Y., K.Y., I.-F.H., Y.L., X.-H.D., C.L., Y.X., H.-F.W., A.-C.S., R.-M.H., and W.-B.Z. performed research; X.Y., K.Y., I.-F.H., Y.L., X.-H.D., C.L., Y.X., H.-F.W., A.-C.S., G.R.N., R.-M.H., E.-Q.C., W.-B.Z., and S.Z.D.C. analyzed data; and X.Y., K.Y., I.-F.H., Y.L., X.-H.D., C.L., Y.X., H.-F.W., A.-C.S., G.R.N., R.-M.H., E.-Q.C., W.-B.Z., and S.Z.D.C. wrote the paper.

Conflict of interest statement: The authors are declared to be the inventors of a provisional patent application filed by the University of Akron related to the results reported here.

*This Direct Submission article had a prearranged editor.

[1]X.Y. and K.Y. contributed equally to this work.

[2]To whom correspondence may be addressed. E-mail: scheng@uakron.edu, eqchen@pku.edu.cn, or wz8@uakron.edu.

This article contains supporting information online at www.pnas.org/lookup/suppl/doi:10.1073/pnas.1302606110/-/DCSupplemental.

can be designed using shape- and volume-persistent nanoparticles as the polar heads and polymer chains of distinct composition and architectures as the tails. Such polymer-tethered nanoparticles have also been proposed as prototype shape amphiphiles. Although computational modeling has predicted versatile phase behaviors and unique self-assembled morphologies (31–33), the potential of this class of materials has remained largely unexplored experimentally due to the difficulty in their precise synthesis in large quantity (34). Compact and rigid molecular nanoparticles (MNPs) with specific symmetry and precise structure provide access to perfect building blocks for the polar heads (30, 35, 36). They include, but are not limited to, polyhedral oligomeric silsesquioxane (POSS) (37, 38) and [60]fullerene (C_{60}) (39, 40) derivatives. In this paper, we report MNP-based giant surfactants (Fig. 1*A*), as unique materials that can generate self-assembled nanostructures with sub-10-nm feature sizes in the bulk, thin film, and solution states. Not only do they exhibit a unique duality of small-molecule surfactants and block copolymers, but also they display diverse morphologies that are of significant technological relevance.

Results and Discussion

If we consider MNPs as the polar heads, various giant surfactants can be constructed in analogy to their small-molecule surfactant counterparts, as schematically illustrated in Fig. 1*A*. Notably, the head groups can be different MNPs with patchy surface chemistry; whereas the tails can vary in chemical composition and chain topology, both of which greatly diversify the molecular design and provide endless possibilities in fine-tuning their structural formations. Extensive libraries of giant surfactants have been synthesized (41–44) and screened for their self-assembled morphologies in the bulk, thin film, and solution states, as outlined in *SI Text*. Following the "click" philosophy, the syntheses of these giant surfactants fulfill an assembly process that is modular, robust, and efficient (45). Not only can each of the materials be readily synthesized in gram quantities, but also the molecular parameters (such as the identity of periphery functional groups on MNPs and the length of polymer tails) can be individually tailored and systematically varied. The chemical structures of five exemplary giant surfactant libraries are shown in Fig. 1*B*, their synthetic approaches are shown in Schemes S1–S5, and their molecular characterizations are summarized in Table S1. In the present study, all of the polymer tails are hydrophobic polystyrene (PS). It should be noted that they can also vary from a wide range of selections (42). It is equally expected that the introduction of other chemically incompatible polymers with competing interactions would further enrich the palette and drive the formation of unique hierarchical structures.

In the bulk, these giant surfactants readily undergo microphase separation and self-assemble into various ordered morphologies at the nanometer scale. Owing to the high diffusion mobility of MNP heads and the lack of chain entanglement in the relatively low molecular weight (MW) region of polymer tails, they exhibit rapid self-assembly dynamics and achieve thermodynamically stable phases typically within minutes to hours upon thermal annealing. Fig. 2*A* shows a set of one-dimensional (1D) small-angle X-ray scattering (SAXS) profiles in reciprocal space obtained from a subset of samples in library 1, DPOSS-PS_n, where DPOSS represents hydroxyl-functionalized POSS and n denotes the average degree of polymerization of PS with different lengths. With increasing PS tail length (also the volume fraction of PS, V_{PS}, Table S1), the self-assembled structures change from lamellae (Lam), to double gyroids (DG), to hexagonally packed cylinders (Hex), and further to body-centered cubic spheres (BCC). This is in good agreement with the observation of microtomed thin sections of the bulk samples in real

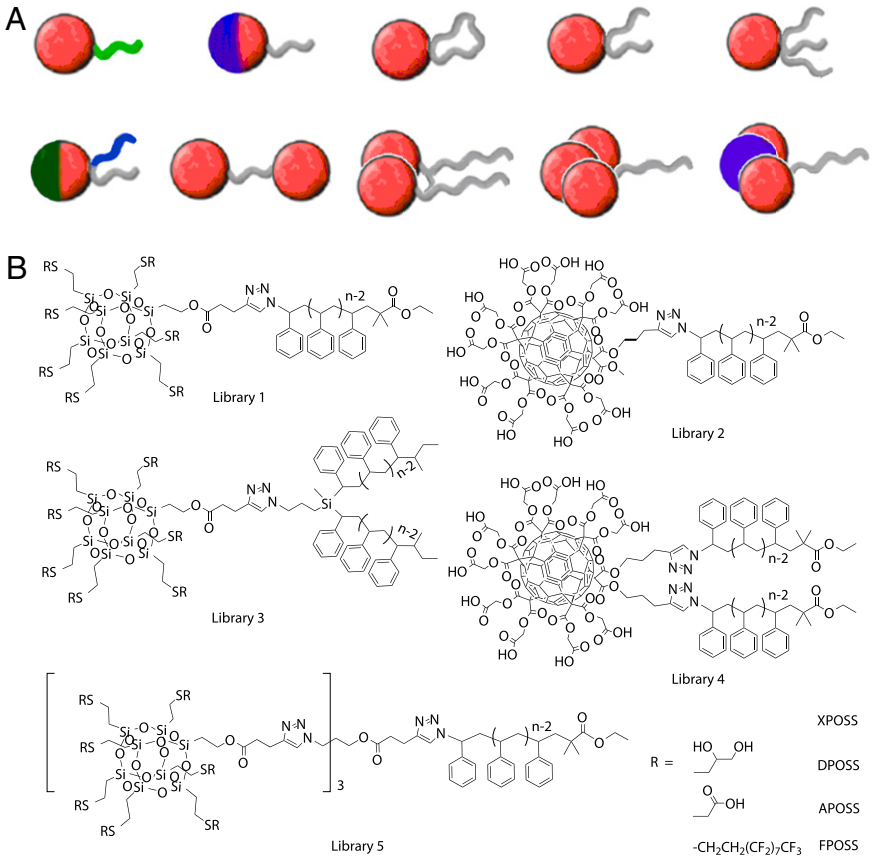

Fig. 1. Cartoon illustration of various giant surfactants and representative libraries studied in this work. (*A*) Cartoon illustration of typical giant surfactants, including (*Left* to *Right*, *Top* to *Bottom*) normal giant surfactant, patchy giant surfactant, necklace-like giant surfactant, giant lipid, multitailed giant surfactant, hybrid giant surfactant, giant bolaform surfactant, giant gemini surfactant, multiheaded giant surfactant, and hetero-headed giant surfactant. (*B*) Library 1 refers to XPOSS-PS_n, where X denotes the functional groups on POSS (D for hydroxyls, A for carboxylic acids, and F for perfluorinated chains). Library 2 refers to AC_{60}-PS_n. Library 3 refers to XPOSS-2PS_n, where the attachment of two identical tails to a junction point introduces a topological effect. Library 4 refers to AC_{60}-2PS_n, which could be topological isomers to library 2. Library 5 refers to a series of multiheaded surfactants, 3XPOSS-PS_n.

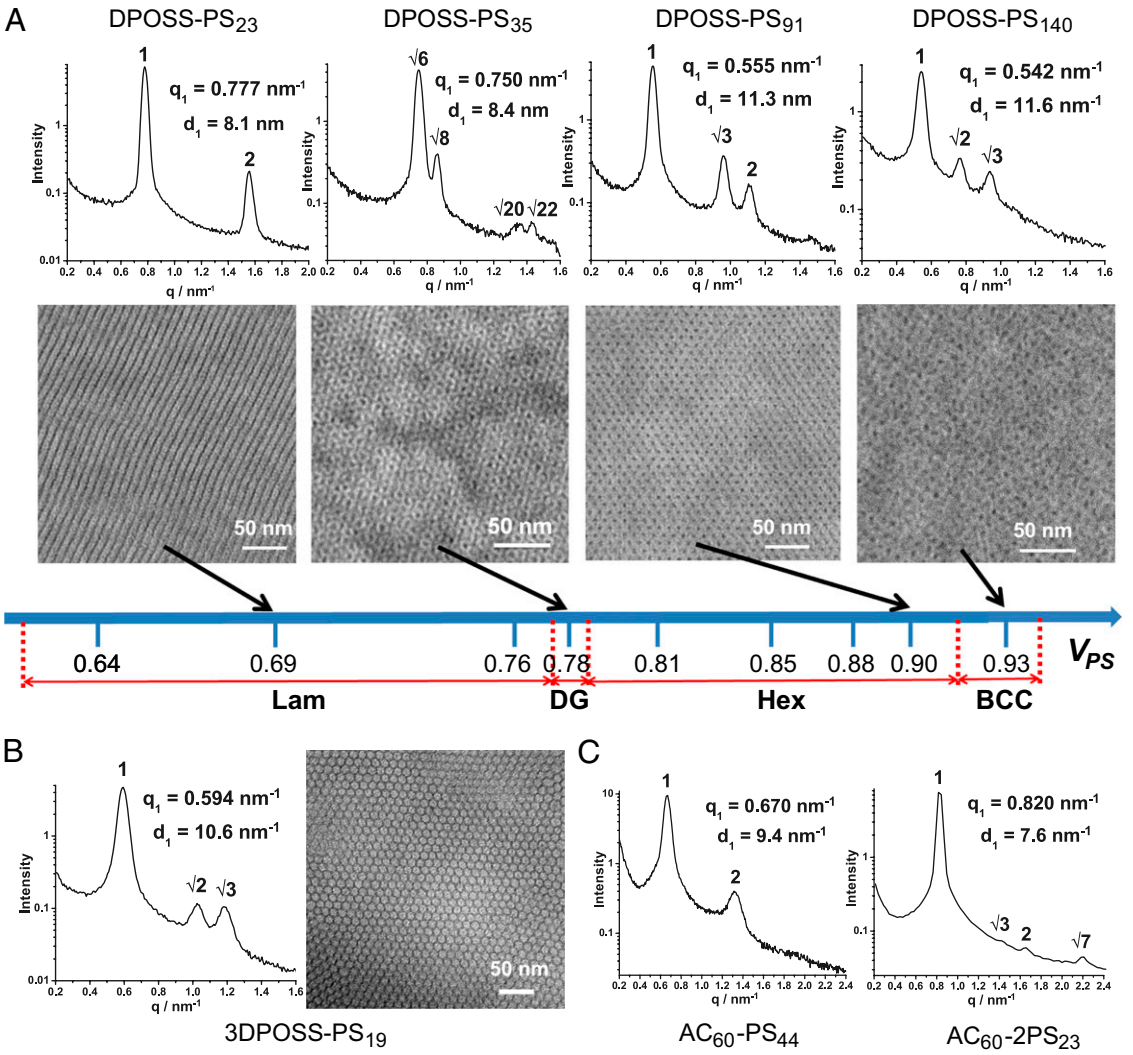

Fig. 2. One-dimensional SAXS profiles and TEM bright-field mass-thickness-contrast images of the giant surfactant samples. (*A*) One-dimensional SAXS profiles (*Upper*) and TEM images (*Lower*) for samples DPOSS-PS_n: (*Left* to *Right*) DPOSS-PS_{23} in lamella (Lam) phase, DPOSS-PS_{35} in double-gyroids (DG) phase, DPOSS-PS_{91} in hexagonally packed cylinder (Hex) phase, and DPOSS-PS_{140} in body-centered cubic sphere (BCC) phase. The POSS domains appear darker than the PS domains. The light blue axis below shows a brief phase diagram of these samples vs. the volume fraction of PS chains (V_{PS}). The black arrows indicate the corresponding V_{PS} values of the samples. The red dashed lines across the axis indicate the estimated boundaries between phases, where the V_{PS} values of observed data points are denoted. From the experimental data of DPOSS-PS_n, the Lam phase appears at least from 64 vol% to 76 vol% of PS, the DG exists around 78 vol%, the Hex is in between 81 vol% and 90 vol%, and finally the BCC is located around 93 vol%. (*B*) One-dimensional SAXS profile (*Left*) and TEM image (*Right*) of the inverse Hex phase from a multiheaded giant surfactant 3DPOSS-PS_{19} in library 5. (*C*) One-dimensional SAXS profiles obtained from two topological isomers of AC_{60}-PS_{44} in library 2 and AC_{60}-$2PS_{23}$ in library 4. Whereas AC_{60}-PS_{44} exhibits a Lam phase, AC_{60}-$2PS_{23}$ shows a Hex phase.

space under bright-field transmission electron microcopy (TEM). Even for the sample with the lowest MW of PS tail in this series (*ca*. 2.0 kg/mol), the microphase separated lamellar structure exhibits excellent orders and sharp interfaces, supported by the autocorrelation function analysis applied to the corresponding SAXS profile (Fig. S1). Notably all of these patterns were obtained without staining, indicating a high electron density contrast. The trend of this phase structure changes is also followed in the other two series of giant surfactants in library 1 with different head surface functional groups [carboxylic acids (APOSS-PS_n) and perfluorinated alkyl chains (FPOSS-PS_n)] and those in library 2 with a different MNP head group based on carboxylic acid-functionalized C_{60}. The feature sizes of all these samples are typically around 10 nm or smaller (Fig. 2 and Table S1).

Owing to the fixed and relatively small sizes of the head groups, only half of the structural phase diagram is observed in Fig. 2*A*. The lower limit of V_{PS} in libraries 1 and 2 is determined by the shortest PS with narrow dispersity (<1.10). At lower PS MWs, the phase structures are obscured by the increasing dispersity of the PS tails. A precise determination of the other half of the phase diagram would require well-defined oligomers. The structures could also be tuned by adding tails or heads to adjust the constraints on the interfacial curvatures as shown in Fig. 1*A* and more specifically in libraries 3–5. For example, a multiheaded giant surfactant with a low-MW PS tail, such as 3DPOSS-PS_{19} in library 5, exhibits an inverse Hex phase shown in Fig. 2*B*, which has not yet been observed in the single-headed/single-tailed giant surfactant library.

On the other hand, using a different number of tails leads to topological isomers that have identical V_{PS} but distinct polymer topologies (e.g., one head/tail vs. multiple head/tails). An exceptional sensitivity of the resulting phase structure to molecular topology was observed, as demonstrated in two pairs of topological isomers, AC_{60}-PS_{44} (a Lam) and AC_{60}-$2PS_{23}$ (a Hex), as well as

DPOSS-PS_{35} (a DG) and DPOSS-$2PS_{17}$ (a Hex) (Fig. 2*C* and Fig. S2). Therefore, an additional order parameter, the geometric cross-sectional area ratio between the head(s) and tail(s), should be introduced in determining the phase structures. This structural sensitivity is characteristic of small molecules but less significant in block copolymers. Further structural variations, such as using patchy heads or installing heads of different surface functionalities at each end of the polymer chain to create a giant bolaform surfactant, an analog of multiblock copolymers, offer unparalleled opportunities for nanostructure engineering at a sub-10-nm scale.

These self-assembled structures of giant surfactants in the bulk state immediately suggest their potential applications in thin-film nanopatterning. The understanding of thin-film physics has greatly advanced the block copolymer lithography over the past decade, but with feature sizes typically of 20–100 nm (4, 27, 46). The direct generation of laterally long-range ordered, densely packed, defect-free, device-oriented nanostructures (47) possessing sub-20-nm feature sizes and sharp interfacial line edges is a grand challenge in microelectronics to keep pace with the prediction of Moore's law (48). Giant surfactants are perfect candidates to address these issues because, besides the proper feature sizes, the conformational rigidity and chemical monodispersity of the MNP heads would probably limit the line edge roughness, whereas the inorganic silicon–oxygen backbones of the POSS heads would increase the etch contrast between two phase domains. Moreover, the fast self-assembly dynamics of these materials could potentially facilitate the formation of long-range ordered nanostructures having low defect density via solvent or even simple thermal annealing within relatively short times. The latter thermal process is ideal for industrial applications. Furthermore, the shape and volume persistency of the heads might impose packing constraints under confined environments (such as thin films), thus providing access to unconventional nanopatterns.

DPOSS-PS_{35} that exhibits a DG nanostructure in the bulk state was first studied in thin films. As shown in the TEM image of Fig. 3*A*, the thin film of DPOSS-PS_{35} after solvent annealing displays a line pattern. The dark lines with width of *ca*. 2.5 nm correspond to the DPOSS domains, which are anticipated to be composed of two layers of DPOSS MNPs held head-to-head by collective hydrogen bonding. The grazing-incidence small-angle X-ray scattering (GISAXS) pattern (Fig. 3*A*, *Inset*) indicates a Hex structure in thin-film state, in which the cylinders preferentially orient along the {10} plane, parallel to the film substrate (49). The calculated spacing between cylinders based on the GISAXS result is *ca*. 11.0 nm, matching well with the TEM observations, from which the line spacing is determined to be *ca*. 6.0 nm due to the superposition of multiple layers of cylinders. The observed morphological transition from DG in the bulk to Hex in the thin film for DPOSS-PS_{35} is due to the thin-film confinement. Using a similar procedure, the APOSS-PS_{75} sample with a BCC structure in the bulk (Table S1) shows a rectangular dot pattern (Fig. 3*B*) under TEM. These dark spherical dots are APOSS domains with a diameter of *ca*. 4.0 nm. In-plane symmetry is analyzed on the basis of the ratio between the two in-plane vectors a_1 (the second-nearest neighbor) and a_2 (the first-nearest neighbor), following the method previously reported (50). The value of a_1/a_2 is determined to be 1.14 for the APOSS-PS_{75} thin film on the basis of the GISAXS result shown in Fig. 3*B*. This value reveals that the POSS spherical domains pack into a face-centered orthorhombic (FCO) lattice, which possesses in-plane symmetry intermediate in between the hexagonal lattice ($a_1/a_2 = 1$) and BCC {110} plane ($a_1/a_2 = 1.154$) (50, 51). The assembled rectangular arrays conform to the industry-standard rectilinear coordinate systems. These observations promise giant surfactants as emerging nanomaterials for nanostructure fabrication in the field of microelectronics.

Whereas the self-assembly of giant surfactants in the bulk and thin-film states is similar to that of block copolymers, they behave like small-molecule surfactants in solution (30, 40, 52). Not only do they exhibit various micellar morphologies, but also the polymer tails are found to be highly stretched under certain circumstances, a feature reminiscent of small-molecule surfactants. In addition, unusual nanostructured colloidal particles have also been observed from compounds in libraries 2 and 4 by slow addition of a selective solvent, e.g., water, into their solution in 1,4-dioxane. A large difference exists between the colloidal particles obtained from a pair of topological isomers, AC_{60}-PS_{44} and AC_{60}-$2PS_{23}$. Dynamic light scattering (DLS) shows a unimodal narrow size distribution for the formed particles with sizes centered at 220 nm for AC_{60}-PS_{44} and 140 nm for AC_{60}-$2PS_{23}$, respectively (Fig. S3). Scanning electron microscopy (SEM) and TEM bright-field images indicate that spherical colloidal particles are formed from AC_{60}-PS_{44} (Fig. 4 *A*–*C*) and double-truncated conical particles from AC_{60}-$2PS_{23}$ (Fig. 4 *D*–*F*). Tilting SEM experiments confirm the shape of particles (Fig. S4). A zoom-in view of the particles in the TEM further shows an onion-like inner structure in spherical particles (Fig. 4*C*) and a hexagonal inner structure for double-truncated conical particles (Fig. 4*F*). The inner structures are clearly similar to the corresponding bulk structures of these two samples (Fig. 2*C*). These colloidal particles are highly stable in solution, as revealed by their zeta potentials (-57.0 ± 5.5 mV for spherical particles and -60.4 ± 7.8 mV for double-truncated conical particles). It is thus rationalized that the surface of these particles is composed of mainly anionic AC_{60} heads and the bulk portion undergoes further self-organization into various finer nanostructures via phase separation between hydrophilic AC_{60} heads and hydrophobic PS tails. The formation of spherical colloidal particles in solution is probably due to the balance between a smaller bending energy caused by the curvature and a greater gain of

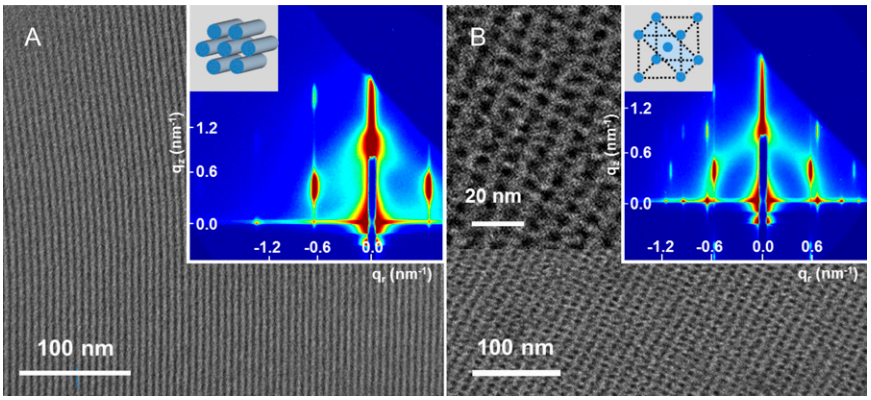

Fig. 3. TEM bright-field mass-thickness-contrast images and GISAXS patterns of two giant surfactant samples in thin-film state. (*A*) TEM image and GISAXS pattern in the reciprocal space of parallel cylindrical Hex structure of DPOSS-PS_{35} thin film. *Inset* shows an illustrated structure in the real space. The dark lines with width of *ca*. 2.5 nm correspond to the DPOSS domains, which are anticipated to be composed of two layers of DPOSS nanoparticles held head-to-head by collective hydrogen bonding. (*B*) TEM image and GISAXS pattern in the reciprocal space of FCO packing a spherical structure of APOSS-PS_{75} thin film. *Inset* shows a zoom-in view of the TEM image and an illustrated structure in the real space. The dots are packed in a rectangular lattice with the sphere diameter of *ca*. 4.0 nm.

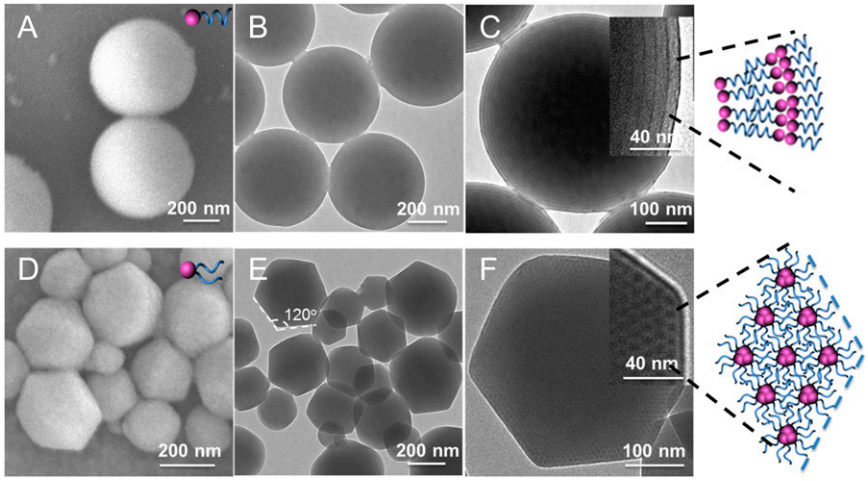

Fig. 4. SEM and TEM images of self-assembled morphologies from two giant surfactants that are topological isomers. (*A* and *B*) SEM (*A*) and TEM (*B*) images of self-assembled morphologies of AC_{60}-PS_{44} in the 1,4-dioxane/water system. (*C*) Zoom-in view shows their inner structures. (*D* and *E*) SEM (*D*) and TEM (*E*) images of self-assembled morphologies of AC_{60}-$2PS_{23}$ under similar conditions. The dark regions are the AC_{60} head domains and the gray regions are the PS tail domains. (*F*) Zoom-in view shows their inner structures.

surface free energy. In contrast, the formation of double-truncated conical particles is most likely dictated by the sixfold symmetry of the close-packed nanostructured cylinders. Although these colloidal particles are reminiscent of "cubosomes" (53), their formation is the result of strong collective hydrogen-bonding interactions and the conformational rigidity of the heads during the self-assembly process, which was not observed in traditional block copolymers.

Conclusions

In conclusion, we have demonstrated by the design, synthesis, and self-assembly of a broad class of giant surfactants that they provide a versatile platform for sub-10-nm nanostructure engineering. As unique additions to the traditional amphiphiles, this class of materials bridges the gap between small-molecule surfactants and block copolymers. They can form diverse structures in the bulk, thin-film, and solution states and exhibit a small-molecule surfactant–block copolymer duality. The self-assembly is found to be sensitive to primary chemical structures in terms of functional groups on MNPs, polymer topology, and chain composition, which suggests possibilities to fine-tune nanostructures through chemical structural variation of the giant surfactants. It should be noted that this class of giant surfactants belongs to an even broader concept of giant molecules and may also be constructed by combining a wide range of nanobuilding blocks and/or structural motifs together, such as MNPs, dendrimers, polymers, and globular proteins, etc. Through structural diversification, this class of materials opens up unique possibilities for macromolecular assemblies.

Materials and Methods

Light Scattering. The DLS experiments were conducted using a Brookhaven Instrument coupled with a Bi-200SM goniometer, a BI-9000AT correlator, and an EMI-9863 photomultiplier tube for photocounting. A Meller Griot 35-mW He-Ne laser was used as light source with wavelength of 632.8 nm. A cylindrical glass scattering cell with diameter of 12 mm was placed at the center of a thermostatic bath (± 0.01 °C). Decahydronaphthalene was used for refractive index matching. Correlation functions at 90° and other angles were recorded at 25 °C. The intensity–intensity time-correlation function $G^{(2)}(t)$ of the distributed object was measured in self-beating mode. It is related to the normalized first-order electric field time correlation function $g^{(1)}(t)$. A Laplace inversion program, CONTIN, was applied to analyze $g^{(1)}(t)$ to obtain the hydrodynamic radius (R_h) as well as its distribution.

Electron Microscopy. A JEOL-1230 microscope with an accelerating voltage of 120 kV was used to record the bright-field images of the TEM. TEM images were taken on a digital CCD camera and processed with the accessory digital imaging system. SEM images were recorded using a JEOL JSM5310 microscope. Silver particles were sputtered on the surface of the sample with a sputter coater (Model ISI 5400) before SEM imaging.

Zeta Potential. The zeta-potential measurement was conducted on a Malvern Instrument (Nano ZS90) equipped with a 632.8-nm He-Ne laser. The instrument calculated the zeta potential by determining the electrophoretic mobility and applying the Henry equation. The electrophoretic mobility was obtained by performing an electrophoresis experiment on the sample and measuring the velocity of the particles using a laser Doppler velocimeter.

SAXS. SAXS experiments were performed on a Rigaku MicroMax 002+ instrument equipped with a 2D multiwire area detector and a sealed copper tube. The working voltage and current for the X-ray tube are 45 kV and 0.88 mA, respectively. The wavelength of the X-ray is 0.154 nm. The scattering vector (q) was calibrated using silver behenate with the primary reflection peak at ($q = 1.067\ nm^{-1}$). The SAXS diffraction patterns covering the q range between 0.2 and 2.0 nm^{-1} were recorded. The recording time for each set of data was 5–10 min, depending on the scattering intensity. The background scattering was subtracted and further analyzed with the Rigaku software SAXSgui.

GISAXS Experiments. GISAXS measurements were performed at the X9 beamline of the National Synchrotron Light Source (NSLS) at Brookhaven National Laboratory. At the NSLS X9 beamline, an incident X-ray beam of energy of 13.5 keV was used.

Preparation of the Bulk Samples for SAXS and Microtomed Samples for TEM. The vacuum-dried powder sample was put into an aluminum sample holder with a hole of 5 mm diameter and sealed with Kapton tapes. The holder was heated to ~120–150 °C under nitrogen atmosphere and annealed at that temperature for 30 min to several hours, depending on the sample conditions. After thermal annealing, the sample was used in SAXS measurements without any other process. Thin slices of the bulk samples were obtained using a Reichert Ultracut S (Leica) microtome on unoriented annealed samples embedded in epoxy monolith at room temperature. The slices were transferred to copper grids coated with amorphous carbon for TEM experiments. The thickness of the slices was around 70–100 nm. For the microtomed samples, in most cases staining is not necessary.

Preparation of Thin-Film Samples and Posttreatment. Thin-film samples were prepared by spin coating the sample solutions in toluene on silicon wafer and carbon-coated silicon wafer or mica. Flat silicon substrates with a 5-nm-thick natural silicon oxide layer were treated with fresh piranha solution at 80 °C for 30 min to form a clean silicon oxide surface, then extensively rinsed with deionized water, and then dried under nitrogen flow. Film thickness was controlled by solution concentration and spin-coating rate. Specifically, for the two samples studied here, the solution concentration was 2.0 wt% and the spin rate was 4,000 rpm. The thin-film thickness is 60.8 nm for DPOSS-PS_{35} and 61.0 nm for APOSS-PS_{75} as determined by spectroscopic ellipsometry. The thin films were further treated by solvent annealing with concentration control. The selected solvent in this study is toluene. Solvent treatment was done by using a home-made apparatus that consisted of two nitrogen lines: one goes through a solvent reservoir and another is pure nitrogen. The solvent concentration

during the treatment is controlled by varying the flow rates of the pure and solvent-infused nitrogen. Thin-film morphology was then investigated by using TEM and GISAXS. All GISAXS experiments were measured under vacuum. The critical angle of both thin-film samples was determined to be around 0.16°, and the incident angle used for both GISAXS measurements was 0.20°. Thin-film samples for the TEM experiment were prepared by spin coating on carbon-coated mica, then immersing the film into water to float it, and then picking it up with a TEM copper gird. Thin-film TEM samples were stained with the vapor of a 4.0-wt% OsO_4 aqueous solution for 1 h to enhance the contrast under TEM. The TEM images of the thin film samples were captured at several spots (>40) that were representative of the whole sample.

Preparation of the Colloidal Particles. A pair of topological isomers, AC_{60}-PS_{44} and AC_{60}-$2PS_{23}$, was dissolved in the common solvent 1,4-dioxane with an initial concentration of 0.02 wt %. Deionized water was gently and slowly added into solution at a rate of 20 μL/min. Water addition was continued until a final water content of 50.0 wt% was reached. At this water content, PS was vitrified and there was no further morphological transformation. Then the colloidal solution was dialyzed against deionized water four times to remove the common solvent and stored for further characterizations. TEM samples were prepared by depositing colloidal solution (10 μL) onto carbon-coated copper grids. After *ca*. 3 min, the excess solution was wicked away by a piece of filter paper. The sample was then allowed to dry under ambient conditions. Twenty microliters of the micelle solution was coated on a silicon wafer and then dried under ambient conditions.

ACKNOWLEDGMENTS. This work was supported by the National Science Foundation (DMR-0906898) and The Joint–Hope Education Foundation.

1. Cheng SZD (2005) Design and engineering of polymer/macromolecular structures on the 2–100 nm length scale: A personal view on structural research. *J Polym Sci B Polym Phys* 43(23):3361–3364.
2. Lin BJ (2004) Immersion lithography and its impact on semiconductor manufacturing. *J Micro/Nanolith MEMS MOEMS* 3(3):377–395.
3. Ash I, Ash M (1980) *Encyclopedia of Surfactants* (Chemical Publishing Company, Revere, MA), pp 1–30.
4. Marencic AP, Register RA (2010) Controlling order in block copolymer thin films for nanopatterning applications. *Annu Rev Chem Biomol Eng* 1:277–297.
5. Percec V, et al. (2010) Self-assembly of Janus dendrimers into uniform dendrimersomes and other complex architectures. *Science* 328(5981):1009–1014.
6. Chen JH, Seeman NC (1991) Synthesis from DNA of a molecule with the connectivity of a cube. *Nature* 350(6319):631–633.
7. Seeman NC (2010) Nanomaterials based on DNA. *Annu Rev Biochem* 79(1):65–87.
8. Hartgerink JD, Beniash E, Stupp SI (2001) Self-assembly and mineralization of peptide-amphiphile nanofibers. *Science* 294(5547):1684–1688.
9. Thomas CS, Glassman MJ, Olsen BD (2011) Solid-state nanostructured materials from self-assembly of a globular protein-polymer diblock copolymer. *ACS Nano* 5(7): 5697–5707.
10. Park SY, et al. (2008) DNA-programmable nanoparticle crystallization. *Nature* 451(7178):553–556.
11. Nykypanchuk D, Maye MM, van der Lelie D, Gang O (2008) DNA-guided crystallization of colloidal nanoparticles. *Nature* 451(7178):549–552.
12. Knorowski C, Travesset A (2011) Materials design by DNA programmed self-assembly. *Curr Opin Solid State Mater Sci* 15(6):262–270.
13. Knorowski C, Burleigh S, Travesset A (2011) Dynamics and statics of DNA-programmable nanoparticle self-assembly and crystallization. *Phys Rev Lett* 106(21): 215501.
14. Whitesides GM, Mathias JP, Seto CT (1991) Molecular self-assembly and nanochemistry: A chemical strategy for the synthesis of nanostructures. *Science* 254(5036): 1312–1319.
15. Whitesides GM, Grzybowski B (2002) Self-assembly at all scales. *Science* 295(5564): 2418–2421.
16. Stang PJ, Olenyuk B (1997) Self-assembly, symmetry, and molecular architecture: Coordination as the motif in the rational design of supramolecular metallacyclic polygons and polyhedra. *Acc Chem Res* 30(12):502–518.
17. Glotzer SC, Solomon MJ (2007) Anisotropy of building blocks and their assembly into complex structures. *Nat Mater* 6(8):557–562.
18. Agarwal U, Escobedo FA (2011) Mesophase behaviour of polyhedral particles. *Nat Mater* 10(3):230–235.
19. Kang H, et al. (2008) Hierarchical assembly of nanoparticle superstructures from block copolymer-nanoparticle composites. *Phys Rev Lett* 100(14):148303.
20. Damasceno PF, Engel M, Glotzer SC (2012) Predictive self-assembly of polyhedra into complex structures. *Science* 337(6093):453–457.
21. Chen Q, Bae SC, Granick S (2011) Directed self-assembly of a colloidal kagome lattice. *Nature* 469(7330):381–384.
22. Wang Y, et al. (2012) Colloids with valence and specific directional bonding. *Nature* 491(7422):51–55.
23. Date RW, Bruce DW (2003) Shape amphiphiles: Mixing rods and disks in liquid crystals. *J Am Chem Soc* 125(30):9012–9013.
24. Glotzer SC (2004) Some assembly required. *Science* 306(5695):419–420.
25. Koga N, et al. (2012) Principles for designing ideal protein structures. *Nature* 491(7423):222–227.
26. Bates FS, Fredrickson GH (1990) Block copolymer thermodynamics: Theory and experiment. *Annu Rev Phys Chem* 41:525–557.
27. Hawker CJ, Russell TP (2005) Block copolymer lithography: Merging "bottom-up" with "top-down" processes. *MRS Bull* 30(12):952–966.
28. Cushen JD, et al. (2012) Oligosaccharide/silicon-containing block copolymers with 5 nm features for lithographic applications. *ACS Nano* 6(4):3424–3433.
29. Tang CB, Lennon EM, Fredrickson GH, Kramer EJ, Hawker CJ (2008) Evolution of block copolymer lithography to highly ordered square arrays. *Science* 322(5900):429–432.
30. Yu XF, et al. (2010) A giant surfactant of polystyrene-(carboxylic acid-functionalized polyhedral oligomeric silsesquioxane) amphiphile with highly stretched polystyrene tails in micellar assemblies. *J Am Chem Soc* 132(47):16741–16744.
31. Zhang ZL, Horsch MA, Lamm MH, Glotzer SC (2003) Tethered nano building blocks: Toward a conceptual framework for nanoparticle self-assembly. *Nano Lett* 3(10): 1341–1346.
32. Glotzer SC, et al. (2005) Self-assembly of anisotropic tethered nanoparticle shape amphiphiles. *Curr Opin Colloid Interface Sci* 10(5–6):287–295.
33. Goyal S, Escobedo FA (2011) Structure and transport properties of polymer grafted nanoparticles. *J Chem Phys* 135(18):184902–184912.
34. Park S, Lim JH, Chung SW, Mirkin CA (2004) Self-assembly of mesoscopic metal-polymer amphiphiles. *Science* 303(5656):348–351.
35. Laine RM (2005) Nanobuilding blocks based on the $[OSiO_{1.5}]_x$ (x = 6, 8, 10) octasilsesquioxanes. *J Mater Chem* 15(35–36):3725–3744.
36. Roll MF, Asuncion MZ, Kampf J, Laine RM (2008) Para-Octaiodophenylsilsesquioxane, $[p\text{-}IC6H4SiO_{(1.5)}]_8$, a nearly perfect nano-building block. *ACS Nano* 2(2):320–326.
37. Li YW, et al. (2011) Breaking symmetry toward nonspherical Janus particles based on polyhedral oligomeric silsesquioxanes: Molecular design, "click" synthesis, and hierarchical structure. *J Am Chem Soc* 133(28):10712–10715.
38. Sun HJ, et al. (2011) Hierarchical structure and polymorphism of a sphere-cubic shape amphiphile based on a polyhedral oligomeric silsesquioxane-[60]fullerene conjugate. *J Mater Chem* 21(37):14240–14247.
39. Zhang WB, et al. (2008) "Clicking" fullerene with polymers: Synthesis of [60]fullerene end-capped polystyrene. *Macromolecules* 41(3):515–517.
40. Yu XF, et al. (2012) Giant molecular shape amphiphiles based on polystyrene-hydrophilic [60]fullerene conjugates: Click synthesis, solution self-assembly, and phase behavior. *J Am Chem Soc* 134(18):7780–7787.
41. He J, et al. (2012) Fluorinated polyhedral oligomeric silsesquioxane-based shape amphiphiles: Molecular design, topological variation, and facile synthesis. *Polym Chem* 3(8):2112–2120.
42. Yue K, et al. (2012) Sequential "click" approach to polyhedral oligomeric silsesquioxane-based shape amphiphiles. *Macromolecules* 45(20):8126–8134.
43. Yue K, et al. (2013) Anionic synthesis of a "clickable" middle-chain azide functionalized polystyrene and its application in shape amphiphiles. *Chin J Polym Sci* 31(1): 71–82.
44. Yue K, et al. (2013) Exploring shape amphiphiles beyond giant surfactants: Molecular design and click synthesis. *Polym Chem* 4(4):1056–1067.
45. Kolb HC, Finn MG, Sharpless KB (2001) Click chemistry: Diverse chemical function from a few good reactions. *Angew Chem Int Ed Engl* 40(11):2004–2021.
46. Park S, et al. (2009) Macroscopic 10-terabit-per-square-inch arrays from block copolymers with lateral order. *Science* 323(5917):1030–1033.
47. Stoykovich MP, et al. (2005) Directed assembly of block copolymer blends into nonregular device-oriented structures. *Science* 308(5727):1442–1446.
48. Black CT, et al. (2007) Polymer self assembly in semiconductor microelectronics. *IBM J Res Develop* 51(5):605–633.
49. Lee B, et al. (2005) Structural analysis of block copolymer thin films with grazing incidence small-angle X-ray scattering. *Macromolecules* 38(10):4311–4323.
50. Stein GE, Kramer EJ, Li X, Wang J (2007) Layering transitions in thin films of spherical-domain block copolymers. *Macromolecules* 40(7):2453–2460.
51. Stein GE, et al. (2007) Symmetry breaking of in-plane order in confined copolymer mesophases. *Phys Rev Lett* 98(15):158302.
52. Wang Z, et al. (2013) Giant gemini surfactants based on polystyrene-hydrophilic polyhedral oligomeric silsesquioxane shape amphiphiles: Sequential "click" chemistry and solution self-assembly. *Chem Sci* 4(3):1345–1352.
53. Almgren M, Edwards K, Karlsson G (2000) Cryo transmission electron microscopy of liposomes and related structures. *Colloids Surf A Physicochem Eng Asp* 174(1–2):3–21.